

## XFEM fracture analysis by applying smoothed weighted functions with compact support

Song-II Ham and Hyon-Sik Hong\*

*Institute of Mechanics, State Academy of Sciences, Pyongyang, DPR of Korea*

---

### ARTICLE INFO

*Article history:*

Received 10 January, 2018

Accepted 29 May 2018

Available online

29 May 2018

---

*Keywords:*

*Crack Analysis*

*XFEM*

*Meshfree Shape Function*

*Smoothed Weighted Function*

*Compact Support*

---

---

### ABSTRACT

In this paper, a smoothed weighted function with the compact support is suggested to improve the numerical accuracy of blending elements for the extended finite element method (XFEM) applied to the crack problem. Such a weight function consists of the shape functions used for the meshless method, reflecting the characteristics of the enriched bases inside the blending element. The effectiveness of this weight function is validated through the numerical examples.

© 2018 Growing Science Ltd. All rights reserved.

## 1. Introduction

Numerical methods for solving discontinuous problems are still being attracted by many researchers in the field of computational fracture mechanics. Instead of traditional finite element method combining with adaptive meshing, many studies have been conducted in order to improve the numerical accuracy of global and local solutions for discontinuous problems (Bittencourt et al., 1996; Bourdin et al., 2000; Hansbo & Hansbo, 2004; Karihalloo & Xiao, 2003; Loehnert & Belytschko, 2007; Miehe & Gurses, 2007; Moës et al., 1999; Oliver, 1989; Areias et al., 2009). Moreover, an efficient method to initiate and propagate cracks in 2D models was offered, independently of the constitutive and element specific technology (Areias et al., 2016; Areias et al., 2015; Areias et al., 2013; Areias & Rabczuk, 2013). Even though these studies are known to be effective for problems accompanying by finite strain, they still use the local remeshing.

XFEM still has challenges for large amplitude displacements (Belytschko & Black, 1999; Melenk & Babuska, 1996; Moës et al., 1999), but it is an effective method for solving crack problems. Nevertheless, XFEM has a disadvantage that the unity of partition does not be satisfied due to the partial enrichment within blending elements.

The blending element has a critical importance for the numerical accuracy and the convergence

\* Corresponding author.

E-mail addresses: [hongs501@yahoo.com](mailto:hongs501@yahoo.com) (H. Hong )

rate of XFEM (Chessa et al., 2003; Sukumar et al., 2001). The blending element has been widely studied by a number of investigators, including the use of the hierarchical and enhanced blending elements (Chessa et al., 2003; Tarancón et al., 2009) or the assumed strain method (Gracie, 2008). In the corrected or modified XFEM approach given in (Fries, 2008), the global enrichment function is localized through the multiplication by the ramp function. All the nodes within the zone where the localized enrichment function is not equal to zero are enriched, leading to the disappearance of enrichment in elements where only some of nodes are enriched. The ramp functions are constructed by the FE shape functions. Chahine et al. (2008) applied such an approach to the crack tip enrichment. Later, Ventura et al. (2009) studied the corrected XFEM more deeply and they called the corrected XFEM as the weighted XFEM. Recently, the partition of unity finite element method (PUFEM) was used to solve the blending element, leading to an optimal convergence rate and a significant improvement of numerical accuracy (Shibamura & Utsunomiya, 2008). But the PUFEM increased the number of degrees of freedom, significantly.

The idea of XFEM was extended into the meshfree method for linear elastic crack problems (Rabczuk & Belytschko, 2004; Ventura et al., 2002; Amiri et al., 2014) and the extended element-free Galerkin (XEFG) was also developed for cohesive cracks (Rabczuk & Zi, 2007). Meanwhile, Fries (2008) developed a new XEFG for removing the blending region and thereafter this method was applied for three-dimensional modeling of crack growth (Timon et al., 2010). The advantage of this XEFG as compared with XFEM is that it has the highly smoothed property, the non-local interpolation property and higher-order continuity, being capable of improving the solution accuracy near the crack tip even though it may have some difficulties in applying Dirichlet boundary condition. Amiri et al. (2014) provided an approach based on local maximum entropy (LME) shape functions along with other functions implemented in partition of unity techniques to discretize problems in linear elastic fracture mechanics. The implementation of LME shape functions does not create any troubles in using the boundary conditions since they meet the Kronecker-Delta property. Moreover, this helps to reach the optimal convergence (same as in FEM) for energy norm and stress intensity factors without special treatment of the nodes close to the crack such as blending or shifting.

In this paper, authors suggest a smoothed weighted function with the compact support in order to improve the numerical accuracy of blending elements for the extended finite element method (XFEM) applied to the crack problem. Such a weight function consists of the shape functions used for the meshless method, reflecting the characteristics of the enriched bases inside the blending element. Such a weight function reproduces the enrichment function in the enriched element similar to the ramp function which Fries (2008) has proposed. The weight function has a value of zero at the non-enriched nodes in the blending element and varies smoothly inside the blending element. Introduction of such a weight function can reflect the local property of discontinuity more accurately and improve the numerical accuracy due to the parasitic terms in blending elements, as demonstrated in numerical validations.

The contents of this paper are as follows. Section 2 gives a brief description of the standard and weighted XFEM. Section 3 considers the accommodation of the meshfree shape functions with a smooth compact support within the finite element. Section 4 explains briefly the extraction of stress intensity factor (SIF) for XFEM. Numerical validations are presented in section 5, followed by a few concluding remarks in section 6.

## 2. Brief description of XFEM

The displacement approximation for the standard XFEM has the following form

$$u^h(\mathbf{x}) = \underbrace{\sum_{i \in I} N_i(\mathbf{x}) u_i}_{\text{Standard FE part}} + \underbrace{\sum_{i \in I^*} M_i(\mathbf{x}) a_i}_{\text{Enriched part}}, \quad (1)$$

where  $I$  is a set containing all nodes in the finite element model and  $M_i(\mathbf{x})$  is the local enrichment function for node  $i$ . The component  $N_i$  is the shape function of the standard finite element method with the node  $i$  and  $u_i$  is the corresponding degree of freedom. Coefficient  $a_i$  is the degree of freedom related to the node  $i$  and  $I^*$  is a subset containing the enriched nodes ( $I^* \subset I$ ). An element with enriched nodal is called as an enriched element. As shown from Fig. 1, so called the geometrical enrichment approach enriches all elements within the area with a radius of  $r$ . In the other hand, the topological enrichment approach enriches only elements containing a crack tip. This study does not consider the topological enrichment since it has lower accuracy and convergence rate than the geometrical enrichment.

Eq. (1) shows that the XFEM displacement approximation consists of the standard FE part and the enriched part. The local enrichment  $M_i(\mathbf{x})$  is expressed as

$$M_i(\mathbf{x}) = N_i^*(\mathbf{x}) \cdot \psi(\mathbf{x}), \quad \forall i \in I^* \quad (2)$$

where  $N_i^*(\mathbf{x})$  is the partition of unity function,

$$\sum_{i \in I^*} N_i^*(\mathbf{x}) = 1 \quad (3)$$

and  $\psi(\mathbf{x})$  is the global enrichment function. The functions  $N_i^*(\mathbf{x})$  are standard FE shape functions that are not necessarily the same as those of the standard part of the approximation (1). In this paper, finite element shape functions with the same order on the standard part as well as the enriched part are used ( $N_i(\mathbf{x}) = N_i^*(\mathbf{x})$ ). For blending elements in which only some of nodes belong to  $I^*$ ,  $\psi(\mathbf{x})$  could not be reproduced exactly due to the lack of partition unity of  $N_i^*(\mathbf{x})$ , whereas the global enrichment function  $\psi(\mathbf{x})$  can be reproduced exactly for any element, in which all nodes belong to  $I^*$ . When all nodes are enriched so that the global enrichment function  $\psi(\mathbf{x})$  is exactly reproduced, such elements are called as reproducing elements.

For blending elements, there are parasitic terms, which could not be compensated by the standard FE part. For example, the displacement approximation for the blending element is constituted as follows (Fig. 1).

$$u^h(\mathbf{x}) = \sum_{i=1}^4 N_i(\mathbf{x}) u_i + N_3^*(\mathbf{x}) \psi(\mathbf{x}) a_3 \quad (4)$$

The parasitic term  $N_3^*(\mathbf{x}) \psi(\mathbf{x}) a_3$  can not be compensated only by the standard FE approximation  $\sum_{i=1}^4 N_i(\mathbf{x}) u_i$  in Eq. (4), leading to poor numerical accuracy and bad convergence.

The displacement approximation of the weighted XFEM has the following form

$$u^h(\mathbf{x}) = \sum_{i \in I} N_i(\mathbf{x}) u_i + \sum_{i \in J^*} N_i^*(\mathbf{x}) \psi(\mathbf{x}) \varphi(\mathbf{x}) a_i \quad (5)$$

where  $\varphi(\mathbf{x})$  is so called the ramp or weight function (Fries, 2008), with the compact support. The weight function is defined only for nodes belonging to  $I^*$  within the enriched zone of the standard XFEM. Thus, if finite element shape functions are used for weight functions, then its value is equal to 1 at enriched nodes and 0 at non-enriched nodes in the blending element. As a result, the parasitic effects of blending elements are removed in the weighted XFEM. Since the weight function is defined at only the nodes belonging to  $I^*$ , the enriched zone could be extended into the blending elements without any change of Eq. (5). As seen from Fig. 2, this zone includes the nodes belonging to  $J^*$ .

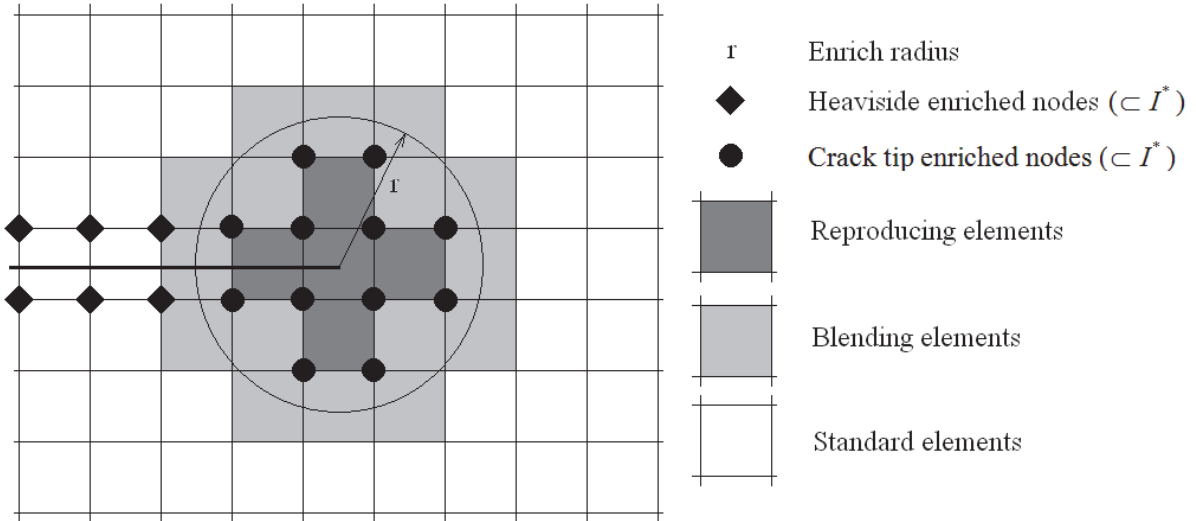


Fig. 1. Enriched elements for the standard XFEM

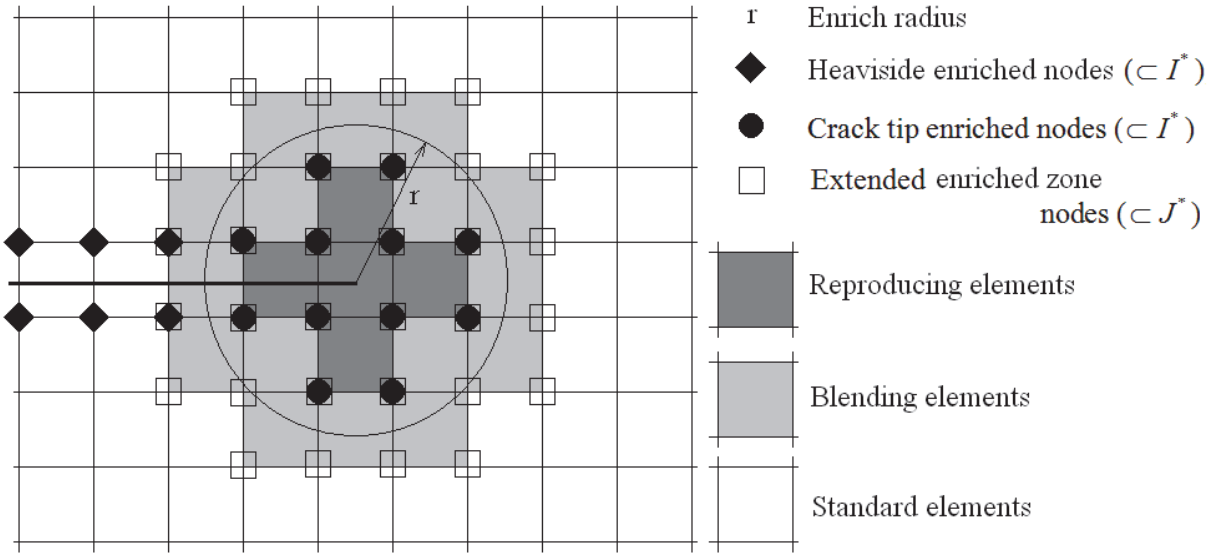


Fig. 2. Extended enriched zones for the corrected XFEM

Fries (2008) used the ramp function as the weight function,

$$\varphi(\mathbf{x}) = \sum_{i \in I^*} N_i^*. \quad (6)$$

Multiplying the weight function by the enrichment function, the global enrichment function  $\psi^{\text{mod}}(\mathbf{x})$  is expressed as,

$$\psi^{\text{mod}}(\mathbf{x}) = \psi(\mathbf{x}) \cdot \varphi(\mathbf{x}) \quad (7)$$

Adopting this global enrichment function  $\psi^{\text{mod}}(\mathbf{x})$ ,  $\psi(\mathbf{x})$  is exactly reproduced in the enriched elements, becomes equal to 0 in the standard elements and varies linearly between 0 and  $\psi(\mathbf{x})$  in the blending elements.

Considering Eq. (7), Eq. (5) can be rewritten as,

$$u^h(\mathbf{x}) = \sum_{i \in I} N_i(\mathbf{x}) u_i + \sum_{i \in J^*} N_i^*(\mathbf{x}) \psi^{\text{mod}}(\mathbf{x}) a_i \quad (8)$$

In this approach, the weight function is used to remove the parasitic terms by constituting the partition of unity in the blending elements. In general, the discontinuous property decreases as it goes away from the discontinuity. Such tendency can be considered by the variation of the global enrichment function  $\psi(\mathbf{x})$  in the enriched part of the XFEM approximation. It should be noted that the variation tendency of enriched functions could be controlled by using generalized weighted functions such as the monotonic decreasing functions with the compact support. For such weighted functions, it would be appropriate to choose the meshfree shape functions having properties similar to ones of FE shape functions.

### 3. Radial point interpolation method (RPIM) based weight function for XFEM

In this section, RPIM meshfree shape functions with the smooth compact support are suggested in order to control the variation of enrichment function inside the blending element. Meshfree shape functions could be mainly divided in ones based on the integration such as SPH method (Smoothed Particle Hydrodynamics), RKPM (Reproducing Kernel Particle Method) and GKR (General Kernel Reproduction Method) and ones based on the series including MLS (Moving Least Squares) method, PIM (Point Interpolation Method) and RPIM (Radial Point Interpolation Method) (Wendland, 1995). Among them, SPH, RKPM, GKR and MLS could not reproduce the enrichment function exactly since they do not satisfy the Kronecker-Delta function property and may not have positivity. In the meantime, PIM and RPIM shape functions overcome these disadvantages and have advantages of finite element shape functions such as the unity of partition, the Kronecker-Delta function property, the consistency, the reproduce property and the compactness of support zone. Nevertheless, PIM shape functions may cause the singular moment matrix (Eq. (15)) in some case. Thus, we propose the RPIM shape function based on the expression of polynomial for the weight function. Of course, LME meshfree shape functions proposed by Amiri et al. (2014) may be also a good choice for the weight function.

#### 3.1. Radial point interpolation method (RPIM)

The displacement  $u(\mathbf{x})$  based on the RPIM approximation can be written as,

$$u(\mathbf{x}) = \sum_{i=1}^n R_i(\mathbf{x})a_i + \sum_{j=1}^m p_j(\mathbf{x})b_j = \mathbf{R}^T(\mathbf{x})\mathbf{a} + \mathbf{p}^T(\mathbf{x})\mathbf{b} \quad (9)$$

where  $R_i(\mathbf{x})$  is the radial base function (RBF),  $p_j(\mathbf{x})$  is the polynomial basis function,  $\mathbf{x}^T = [x, y]$ ,  $n$  is the number of RBFs and  $m$  is the number of polynomial terms (Liu & Gu, 2005). If  $m = 0$ , only the RBFs are used. Otherwise, RBFs could be extended by  $m$  basis functions. Coefficients  $a_i$  and  $b_j$  are unknown constants.

For the radial basis function  $R_i(\mathbf{x})$ , the distance from  $\mathbf{x}$  to  $\mathbf{x}_i$  is expressed as,

$$r = \sqrt{(x - x_i)^2 + (y - y_i)^2} \quad (10)$$

Multi-quadratic function (Kansa, 1990), the Gaussian function (Sharan et al., 1997), the thin plate spline and the logarithm function (Franke & Schaback, 1997) and the compactly supported RBFs (Wendland, 1995; Wu, 1995) have been used in several studies. Adding the polynomial into Eq. (9) ensures the interpolation stability and the reproducibility.

In order to determine coefficients  $a_i$  and  $b_i$  in Eq. (9), a support domain should be assigned for each node or Gaussian point. The support could contain  $n$  nodes. Coefficient  $a_i$  and  $b_i$  can be determined from

$$\mathbf{U}_s = \mathbf{R}_0 \mathbf{a} + \mathbf{P}_m \mathbf{b} \quad (11)$$

where vector  $\mathbf{U}_s$  represents the nodal degrees of freedom,

$$\mathbf{U}_s = \{u_1 \ u_2 \ \dots \ u_n\}^T \quad (12)$$

and the moment matrix  $\mathbf{R}_0$ ,

$$\mathbf{R}_0 = \begin{bmatrix} R_1(r_1) & R_2(r_1) & \cdots & R_n(r_1) \\ R_1(r_2) & R_2(r_2) & \cdots & R_n(r_2) \\ \cdots & \cdots & \cdots & \cdots \\ R_1(r_n) & R_2(r_n) & \cdots & R_n(r_n) \end{bmatrix}_{(n \times n)} \quad (13)$$

where  $r_k$  is defined as,

$$r_k = \sqrt{(x_k - x_i)^2 + (y_k - y_i)^2} \quad (14)$$

and the polynomial moment matrix is represented as,

$$\mathbf{P}_m^T = \begin{bmatrix} 1 & 1 & \cdots & 1 \\ x_1 & x_2 & \cdots & x_n \\ y_1 & y_2 & \cdots & y_n \\ \vdots & \vdots & \ddots & \vdots \\ p_m(\mathbf{x}_1) & p_m(\mathbf{x}_2) & \cdots & p_m(\mathbf{x}_n) \end{bmatrix}_{(m \times n)} \quad (15)$$

The coefficient vector for the RBF part is stated as

$$\mathbf{a}^T = \{a_1 \ a_2 \ \dots \ a_n\} \quad (16)$$

and the coefficient vector for the polynomial part is expressed as,

$$\mathbf{b}^T = \{b_1 \ b_2 \ \dots \ b_m\}. \quad (17)$$

$n+m$  unknowns of Eq. (11) require additional equations as,

$$\sum_{i=1}^n p_j(\mathbf{x}_i) a_i = \mathbf{P}_m^T \mathbf{a} = 0, \quad j = 1, 2, \dots, m \quad (18)$$

Combination of Eq. (11) with Eq. (18) leads to the following equation

$$\widetilde{\mathbf{U}}_s = \begin{bmatrix} \mathbf{U}_s \\ \mathbf{0} \end{bmatrix} = \underbrace{\begin{bmatrix} \mathbf{R}_0 & \mathbf{P}_m \\ \mathbf{P}_m^T & \mathbf{0} \end{bmatrix}}_G \begin{Bmatrix} \mathbf{a} \\ \mathbf{b} \end{Bmatrix} = \mathbf{G} \mathbf{a}_0 \quad (19)$$

where

$$\mathbf{a}_0^T = \{a_1 \ a_2 \ \dots \ a_n \ b_1 \ b_2 \ \dots \ b_m\}, \quad (20)$$

$$\widetilde{\mathbf{U}}_s = \{u_1 \ u_2 \ \dots \ u_n \ 0 \ 0 \ \dots \ 0\} \quad (21)$$

where  $\mathbf{R}_0$  and  $\mathbf{G}$  are symmetric matrices.

Solving Eq. (19), one can obtain the following expression.

$$\mathbf{a}_0 = \begin{Bmatrix} \mathbf{a} \\ \mathbf{b} \end{Bmatrix} = \mathbf{G}^{-1} \widetilde{\mathbf{U}}_s \quad (22)$$

Eq. (9) could be rewritten as,

$$u(\mathbf{x}) = \mathbf{R}^T(\mathbf{x}) \mathbf{a} + \mathbf{p}^T(\mathbf{x}) \mathbf{b} = \{\mathbf{R}^T(\mathbf{x}) \ \ \mathbf{p}^T(\mathbf{x})\} \begin{Bmatrix} \mathbf{a} \\ \mathbf{b} \end{Bmatrix} \quad (23)$$

or

$$u(\mathbf{x}) = \{\mathbf{R}^T(\mathbf{x}) \quad \mathbf{p}^T(\mathbf{x})\} \mathbf{G}^{-1} \tilde{\mathbf{U}}_s = \bar{\Phi}^T(\mathbf{x}) \tilde{\mathbf{U}}_s \quad (24)$$

where, the RPIM shape function could be expressed as,

$$\tilde{\Phi}^T(\mathbf{x}) = \{\mathbf{R}^T(\mathbf{x}) \quad \mathbf{p}^T(\mathbf{x})\} \mathbf{G}^{-1} = \{\phi_1(\mathbf{x}) \quad \phi_2(\mathbf{x}) \quad \dots \quad \phi_n(\mathbf{x}) \quad \phi_{n+1}(\mathbf{x}) \quad \dots \quad \phi_{n+m}(\mathbf{x})\}. \quad (25)$$

Lastly, the RPIM shape function corresponding to the nodal displacement vector  $\Phi(\mathbf{x})$  can be expressed as,

$$\Phi^T(\mathbf{x}) = \{\phi_1(\mathbf{x}) \quad \phi_2(\mathbf{x}) \quad \dots \quad \phi_n(\mathbf{x})\}. \quad (26)$$

Then, Eq. (24) can be rewritten as,

$$u(\mathbf{x}) = \Phi^T(\mathbf{x}) \mathbf{U}_s = \sum_{i=1}^n \phi_i u_i \quad (27)$$

Derivatives of  $u(\mathbf{x})$  can be easily obtained as

$$u_{,l}(\mathbf{x}) = \Phi_{,l}^T(\mathbf{x}) \mathbf{U}_s \quad (28)$$

where subscript  $l$  denotes the coordinate  $x$  or  $y$  and the comma represents the partial differentiation with respect to the spatial coordinate.

It should be noted that the existence of  $\mathbf{R}_0^{-1}$  has been demonstrated for arbitrary discrete points (Wendland, 1998).

### 3.2. XFEM by using the weight function having the smooth compact support

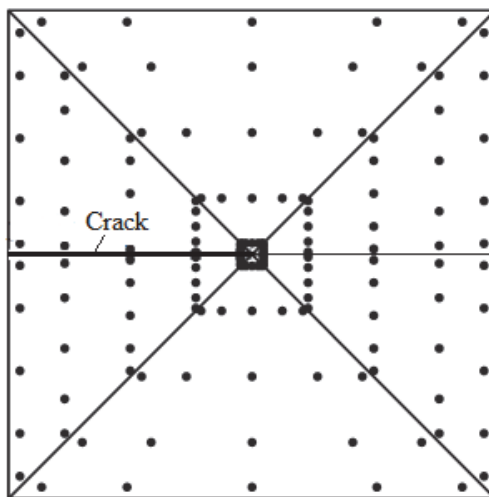
The RPIM shape functions can be used as the weight function of the weighted XFEM. For every node, the support is restricted to one element. For a rectangular support domain, the following RBFs are adopted

$$R_i(x, y) = \left(1 - \frac{\mathbf{x}_i}{h_x}\right)^8 \left(1 + 8 \frac{\mathbf{x}_i}{h_x} + 25 \frac{\mathbf{x}_i^2}{h_x^2} + 32 \frac{\mathbf{x}_i^3}{h_x^3}\right) \cdot \left(1 - \frac{\mathbf{y}_i}{h_y}\right)^8 \left(1 + 8 \frac{\mathbf{y}_i}{h_y} + 25 \frac{\mathbf{y}_i^2}{h_y^2} + 32 \frac{\mathbf{y}_i^3}{h_y^3}\right) \quad (29)$$

where  $h_x$  and  $h_y$  are the size in the  $x$  and  $y$  directions, respectively, and  $\mathbf{x}_i$  and  $\mathbf{y}_i$  are defined as,

$$\mathbf{x}_i = \|x - x_i\|, \quad \mathbf{y}_i = \|y - y_i\| \quad (30)$$

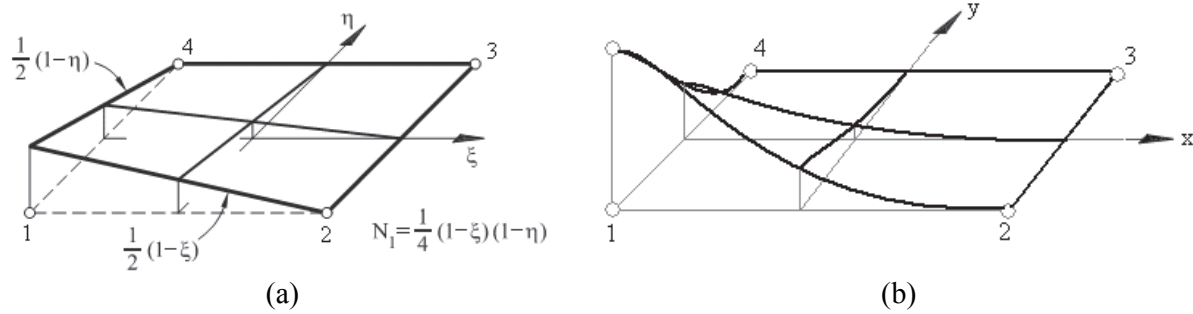
The RPIM shape functions allow for the enrichment function  $\psi(\mathbf{x})$  to be reproduced in the enriched element. In addition, the enrichment function  $\psi(\mathbf{x})$  becomes equal to 0 in the standard element, and varies smoothly between 0 and  $\psi(\mathbf{x})$  in transition elements.



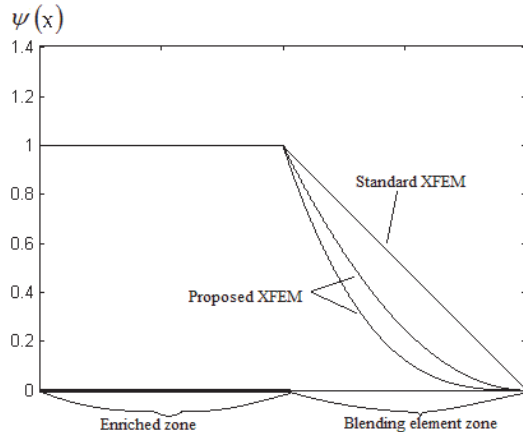
**Fig. 3.** Schematic of numerical integration at an element containing a crack tip

Fig. 3 shows the schematic of numerical integration at the element containing a crack tip. The element containing a crack tip is divided as six triangular sub-areas for numerical integration, each sub-area often having  $5 \times 5$  Gaussian points while blending elements have usually  $5 \times 5$  Gaussian points. Increase of number of integration points may lead to the raise in numerical error, on the contrary. Figs. 4 and 5 also show the variation of the RPIM shape function using the RBF. Integration of weighted function usually follows the standard Gaussian quadrature procedure.

These weight functions could be extended into three-dimensional crack problems without particular numerical difficulties and computational cost may be increased little. For example, the order of radial base functions and the size of moment matrix could be increased for three-dimensional analysis.



**Fig. 4.** Variation of weight functions at 2D for (a) FE shape function and (b) smoothed weight function with compact support.



**Fig. 5.** Variation of weight functions at 1D.

### 3.3. Shifted enrichment function

For the proposed weighted XFEM, a similar shifted formulation to XFEM can be employed: the shifted enrichment for the standard XFEM (Fries, 2008) is,

$$\text{Standard XFEM: } \psi_i^{\text{shift}}(\mathbf{x}) = \psi(\mathbf{x}) - \psi(\mathbf{x}_i), \quad i \in I^* \quad (31)$$

$$\text{Weighted XFEM: } \psi_i^{\text{mod.shift}}(\mathbf{x}) = [\psi(\mathbf{x}) - \psi(\mathbf{x}_i)] \cdot \varphi(\mathbf{x}), \quad i \in J^* \quad (32)$$

Thus, the shifted displacement approximation for the weighted XFEM can be expressed as,

$$u^h(\mathbf{x}) = \sum_{i \in I} N_i(\mathbf{x}) u_i + \sum_{j=1}^m \sum_{i \in J^*} N_i(\mathbf{x}) \cdot [\psi^j(\mathbf{x}) - \psi^j(\mathbf{x}_i)] \cdot \Phi^j(\mathbf{x}) \cdot a_i^j \quad (33)$$

#### 4. Determination of SIFs

The reciprocal integration scheme is used for extraction of SIFs (Chessa et al., 2003),

$$M^{(1,2)} = \int_{\Gamma} \left[ W^{(1,2)} \delta_{ij} - \sigma_{ij}^1 \frac{\partial u_i^{(2)}}{\partial x_j} - \sigma_{ij}^2 \frac{\partial u_i^{(1)}}{\partial x_j} \right] n_j d\Gamma, \quad (34)$$

where  $W^{(1,2)}$  is the interaction strain energy,  $\delta_{ij}$  is the Kronecker-Delta function,  $\sigma_{ij}^1$  and  $\sigma_{ij}^2$  are the stress components for actual and auxiliary states, respectively, and  $u_i^{(1)}$  and  $u_i^{(2)}$  are the displacement components for actual and auxiliary states, respectively.  $\Gamma$  denotes the integration contour and  $n_j$  is the outer normal vector to  $\Gamma$ .

All variables associated with the state 1 are evaluated by XFEM and quantities associated with the state 2 are adopted from the analytical solutions of the crack tip asymptotic field.

The SIFs are then determined by

$$K_i^{(1)} = \frac{E^*}{2} M^{(1,2)}, \quad (35)$$

where  $K_1^{(1)}$  and  $K_2^{(1)}$  are the mode I and II SIFs, respectively and  $E^*$  is the Young's modulus,

$$E^* = \begin{cases} E, & \text{plane stress} \\ \frac{E}{1-\nu^2}, & \text{plane strain} \end{cases} \quad (36)$$

#### 5. Numerical validation

##### 5.1. Mode I and II cracks in an infinite plate under tension

In order to validate the approach suggested in this paper, numerical tests are performed on an infinite plate containing mode I and mode II cracks, and the results of proposed weighted XFEM are compared with the standard XFEM (Fries, 2008).

All examples are assumed in the plane stress state with the Young's modulus of  $E = 2.1 \times 10^{11} N/m^2$  and the Poisson's ratio of  $\nu = 0.3$ . Numerical study is performed on the finite zone near the crack tip of the infinite plate (Fig. 6). The size of zone A ( $2 \times 2$ ) is very small compared with the crack length  $2a$ . The zone A is divided to  $N \times N$  square elements, where  $N$  varies between 9 to 199 and the element size is  $h = 2/N$ . The stiffness matrix and the reciprocal integration are computed by the  $5 \times 5$  Gaussian integration for normal elements and 73-point Gaussian rule for the crack tip elements.

Along the boundary  $\Gamma_A$  of the region A, the asymptotic solution near the crack tip is applied, assuming  $K_I = 1$ ,  $K_{II} = 0$  for the mode I crack and  $K_I = 0$ ,  $K_{II} = 1$  for the mode II crack. The asymptotic solutions near the crack tip for mode I and mode II cracks are stated as

$$\begin{Bmatrix} u_x \\ u_y \end{Bmatrix} = \frac{K_I}{2\mu} \sqrt{\frac{r}{2\pi}} \begin{Bmatrix} \cos \frac{\theta}{2} \left( k - 1 + 2 \sin^2 \frac{\theta}{2} \right) \\ \sin \frac{\theta}{2} \left( k + 1 - 2 \cos^2 \frac{\theta}{2} \right) \end{Bmatrix} \quad (\text{Mode I}) \quad (37)$$

$$\begin{Bmatrix} u_x \\ u_y \end{Bmatrix} = \frac{K_{II}}{2\mu} \sqrt{\frac{r}{2\pi}} \begin{Bmatrix} \sin \frac{\theta}{2} \left( k + 1 + 2 \cos^2 \frac{\theta}{2} \right) \\ -\cos \frac{\theta}{2} \left( k - 1 - 2 \sin^2 \frac{\theta}{2} \right) \end{Bmatrix} \quad (\text{Mode II}) \quad (38)$$

where,  $\mu$  is the shear modulus and  $k$  is the Kolosov's constant (Amiri et al., 2014),

$$k = \begin{cases} 3 - 4\nu & \text{Plane strain} \\ 3 - \nu & \text{Plane strain} \\ 1 + \nu & \end{cases} \quad (39)$$

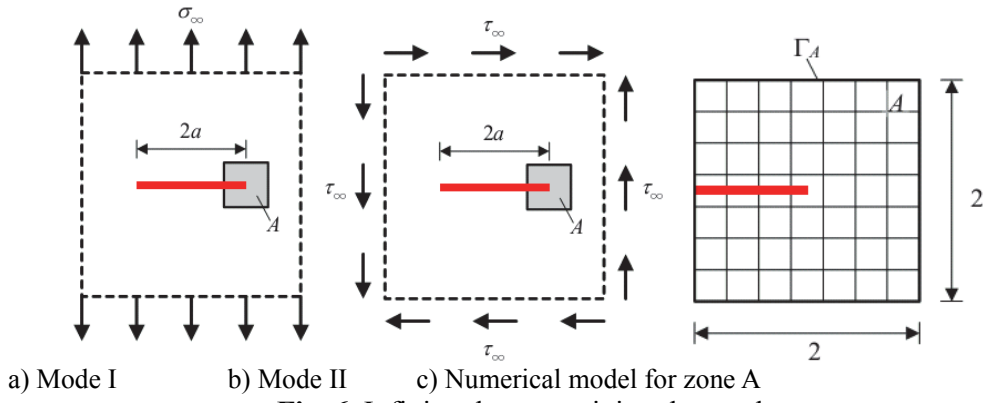


**Fig. 6.** Infinite plate containing the crack.

The size of the enriched zone follows the geometrical enrichment approach. In the present study, all the nodes within a radius of  $R_{tip} = 0.2$  are enriched by Eq. (11). Meanwhile, the SIFs  $K_I$  and  $K_{II}$  are extracted by the evaluation of reciprocal integration on a circular zone with the radius of  $R = 0.6$ . To study the convergence rate, the energy norm is adopted

$$\|\mathbf{e}\| = \|\mathbf{U} - \mathbf{U}^h\| = \frac{\sqrt{\int_A (\boldsymbol{\sigma} - \boldsymbol{\sigma}^h)^T \mathbf{D}^{-1} (\boldsymbol{\sigma} - \boldsymbol{\sigma}^h) dA}}{\sqrt{\int_A \boldsymbol{\sigma}^T \mathbf{D}^{-1} \boldsymbol{\sigma} dA}}, \quad (40)$$

where  $\boldsymbol{\sigma}$  is the analytical solution of stress field near the crack tip and  $\boldsymbol{\sigma}^h$  is the numerical results. Figs 7 to 9 depict the numerical SIFs and energy norms expressed in the logarithm scale, respectively.

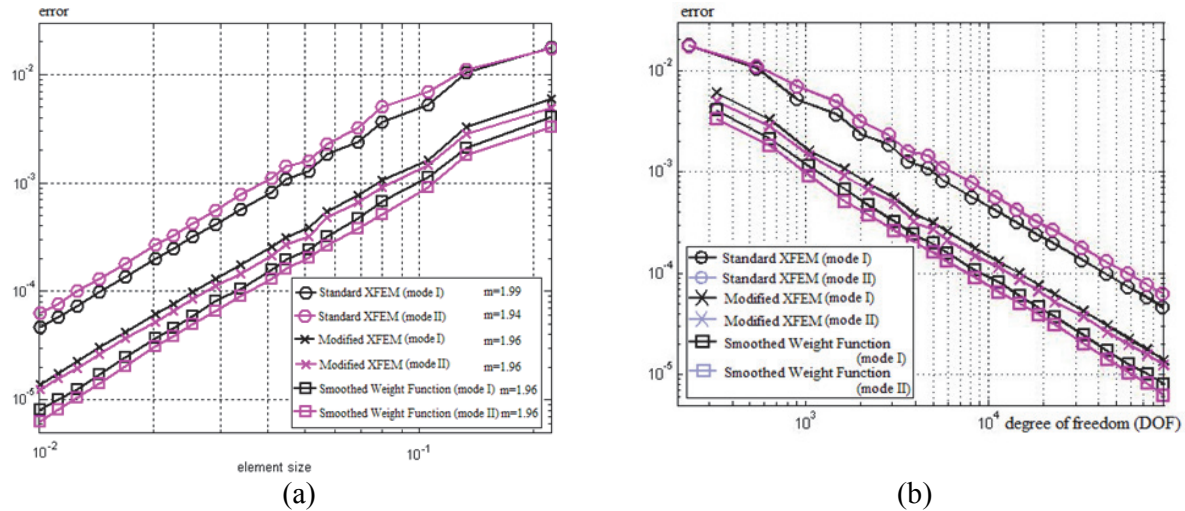


**Fig. 7.** Relative errors of  $K_I$  and  $K_{II}$  (Longitudinal axis is  $|K_i - 1|$ ), a) mesh size vs. error, b) Degrees of freedom (DOF) vs. error

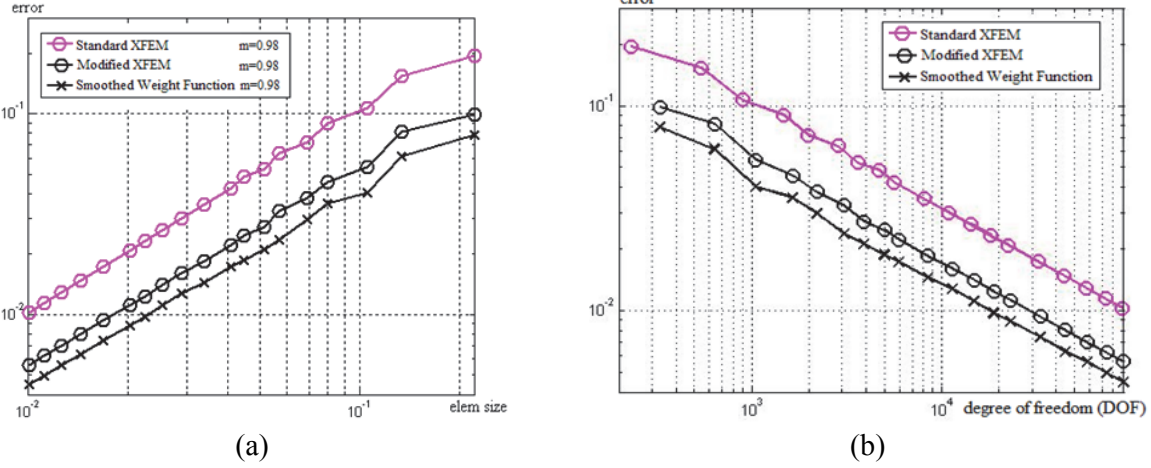


**Fig. 8.** Energy norm of error for mode I, a) mesh size vs. error, b) Degrees of freedom (DOF) vs. error

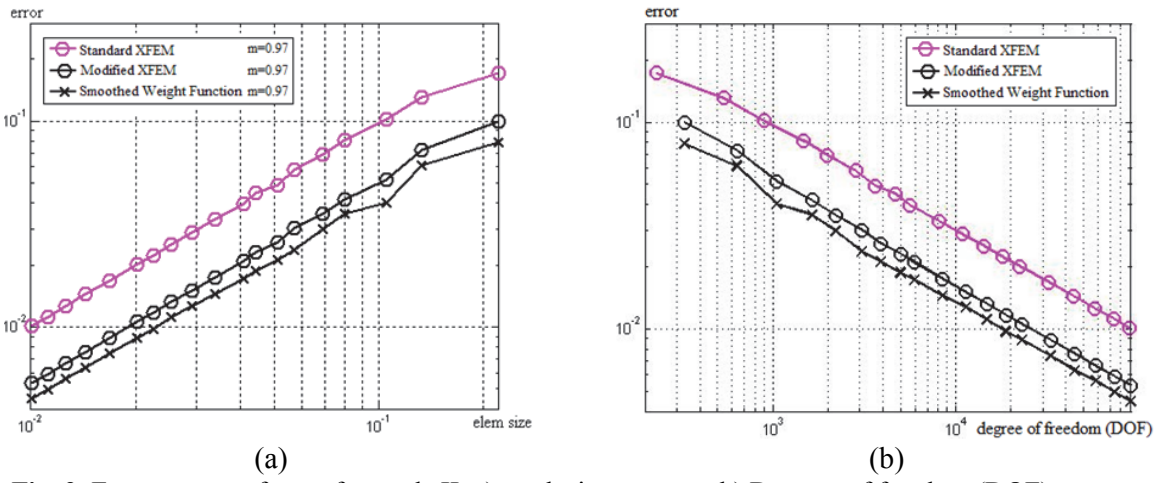


**Fig. 9.** Energy norm of error for mode II, a) mesh size vs. error, b) Degrees of freedom (DOF) vs. error

As shown in Fig. 7, the predicted SIFs converge towards the exact value of 1.0 with the convergence rate of order 2.0 for both modes I and II cracks, and for the same element size and the number of degree of freedom, the introduction of smoothly compacted support improves the numerical accuracy significantly and shows the same convergence rate as in the corrected XFEM (Fries, 2008). This tendency is similarly observed for the energy norm (Figs. 8 and 9).

### 5.2. Enriched meshfree method using LME (Local Maximum Entropy) shape functions

This example was analyzed based on the enriched meshfree method using LME shape function and its result was compared with one in previous section.

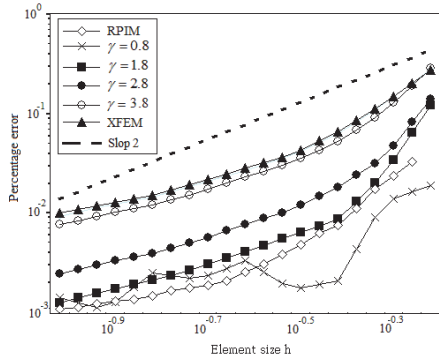


**Fig. 10.** Relative error of SIF with the element size  $h$

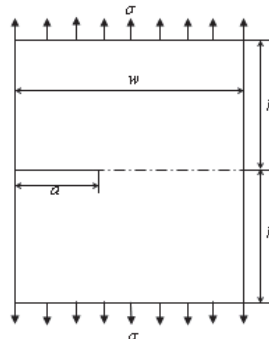


**Fig. 11.** Geometry of SE(T) specimen

The size of zone considered is  $10 \times 10$  and the remaining conditions are the same as in section 5.1. Fig. 10 shows the relative error of SIF with increasing the element size. In Fig. 10,  $\gamma$  denotes the parameter characterizing a degree of locality of LME shape function (Amiri et al., 2014). The current method adopts the RPIM shape function as the weight function while the meshfree method was combined with the LME shape function. As shown from Fig. 10, the current method improve the numerical accuracy than the enriched meshfree method using LME shape function (Amiri et al., 2014) even for the most optimal case of  $\gamma = 1.8$ .

### 5.3. Single notched tension specimen (SE(T))

Fig. 11 shows the geometry of SE(T) specimen. Material properties are the same as in previous case and  $w = 2$ ,  $h = 1.5w$ ,  $a/w = 0.5$  and  $\sigma = 1Pa$  are assumed. The theoretical solution for this problem is equal to  $4.989973 (N/m^{3/2})$  (Erdogan, 2000).

Comparison of the relative error of SIF, computed by the standard XFEM, the modified XFEM (Fries, 2008) and the present weighted XFEM are shown Table 1. Clearly, the present model gives more accurate results.

**Table 1.** Relative errors of SIFs computed by using various approaches.

Methods	Element size						
	2/9	2/11	2/13	2/17	2/19	2/21	2/23
Standard XFEM	6.6966e-2	5.3493e-2	4.3861e-2	2.0361e-2	1.7585e-2	1.536e-2	1.2315e-2
Modified XFEM (Sharan et al., 1997)	1.8343e-2	1.4469e-2	1.1546e-2	3.578e-3	2.82e-3	2.192e-3	1.25e-3
Smoothed Weight Function	1.4346e-2	1.0597e-2	7.837e-3	2.138e-3	1.917e-3	1.503e-3	8.105e-4

As shown from Table 1, the current weight function could improve the numerical accuracy significantly as compared with the standard XFEM and the corrected XFEM. The relative error is reduced 15 times than the standard XFEM and 1.5 times than the corrected XFEM. Even for coarse mesh, the relative error is  $10e-4$ .

## 6. Conclusion remark

In this paper, a smoothed weighted function with the compact support is suggested to improve the numerical accuracy of blending elements for the extended finite element method (XFEM) applied to the crack problem. In general, the weight function is introduced to remove the parasitic terms in blending elements within its support. The weight function, multiplied by the enrichment function, could characterize the variation of enrichment function in blending elements by connecting the standard finite element zone with the enriched zone. Therefore, adjusting the variation of enrichment function between the standard element and the enriched element by using the appropriate weight function, one may improve the numerical accuracy of XFEM. From above considerations, authors suggested a weight function with compact support. By such a weight function, the enrichment function can be exactly reproduced in the enriched elements. It is equal to 0 in the standard elements and varies smoothly inside the blending elements. In other words, it has the same property as for the standard FE shape, but the enrichment function varies non-linearly even for the linear element. Some numerical examples showed that the introduction of current weight functions could improve the numerical accuracy of crack problem even though it does not indicate any improvement of convergence rate. Furthermore, determination of optimal RPIM functions and its extension into three-dimensional problems may reserve future research.

## Acknowledgement

The authors would like to express their deep gratitude to Professor Soheil Mohammadi of University of Tehran, IRAN for giving us valuable comments on this work as well as carefully reviewing this paper.

## References

- Amiri, F., Anitescu, C., Arroyo, M., Bordas, S. P. A., & Rabczuk, T. (2014). XLME interpolants, a seamless bridge between XFEM and enriched meshless methods. *Computational Mechanics*, 53(1), 45-57.
- Areias, P., Msekh, M. A., & Rabczuk, T. (2016). Damage and fracture algorithm using the screened Poisson equation and local remeshing. *Engineering Fracture Mechanics*, 158, 116-143.
- Areias, P., Reinoso, J., & Camanho, P. P (2015). A constitutive-based element by- element crack propagation algorithm with local mesh refinement. *Computational Mechanics*, 56(2), 291-315
- Areias, P., Rabczuk, T., & Dias-da-Costa, D. (2013). Element-wise fracture algorithm based on rotation of edges. *Engineering Fracture Mechanics*, 110, 113-137
- Areias, P., & Rabczuk, T. (2013). Finite strain fracture of plates and shells with configurational forces and edge rotation. *International Journal for Numerical Methods in Engineering*, 94(12), 1099-1122.
- Areias, P., Dias-da-Costa, D., Alfaia, J., & Julio, E. (2009). Arbitrary bi-dimensional finite strain cohesive crack propagation. *Computational Mechanics*, 45(1), 1741-1760.
- Belytschko, T., & Black, T. (1999). Elastic crack growth in finite elements with minimal remeshing. *International Journal for Numerical Methods in Engineering*, 45(5), 601-620.
- Bittencourt, T. N., Ingraffea, A. R., Wawrzynek, P. A., & Sousa, J. L. (1996). Quasi-automatic simulation of crack propagation for 2D LEFM problems. *Engineering Fracture Mechanics*, 55(2), 321-334.
- Bourdin, B., Francfort, G. A., & Marigo, J. -J. (2000). Numerical experiments in revisited brittle fracture. *Journal of Mechanics and Physics of Solids*, 48, 797-826.
- Chahine, E., Laborde, P. & Renard, Y. (2008). Crack tip enrichment in the XFEM using a cutoff function. *International Journal for Numerical Methods in Engineering*, 75, 629-646.
- Chessa, J., Wang, H., Belytschko, T. (2003). On the construction of blending elements for local partition of unity enriched finite elements. *International Journal for Numerical Methods in Engineering*, 57, 1015-1038.
- Erdogan, F. (2000). Fracture mechanics. *International journal of solids and structures*, 37, 171-183.
- Franke, C., & Schaback, R. (1997). Solving Partial Differential Equations by Collocation Using Radial Basis Functions. *Applied Mathematics and Computation*, 93, 73-82.
- Fries, T. P., (2008). A corrected XFEM approximation without problems in blending elements. *International Journal for Numerical Methods in Engineering*, 75, 503-532.
- Goangseup, Z., Timon, R., & Wolfgang, W. (2007). Extended Meshfree Methods without Branch Enrichment for Cohesive Cracks. *Computational Mechanics*, 40(2), 367-382.
- Gracie, R., Wang, H., & Belytschko, T. (2008). Blending in the extended finite element method by discontinuous Galerkin and assumed strain methods. *International Journal for Numerical Methods in Engineering*, 74, 1645-1669.
- Hansbo, A., & Hansbo, P. (2004). A finite element method for the simulation of strong and weak discontinuities in solid mechanics. *Computer Methods in Applied Mechanics and Engineering*, 193, 3523-3540.
- Kansa, E. J. (1990). Multiquadratics-A Scattered Data Approximation Scheme with Applications to Computational Fluid dynamics. *Computers and Mathematical Application*, 19(8/9), 127-145.
- Karihalloo, B. L., & Xiao, Q. Z. (2003). Modeling of stationary and growing cracks in FE framework without remeshing: a state-of-the-art review. *Computational Structure*, 81, 119-129.
- Liu, G. R., & Gu, Y. T. (2005). An introduction to meshfree methods and their programming. Netherlands: Springer.
- Loehnert, S., & Belytschko, T. (2007). A multiscale projection method for macro/microcrack simulations. *International Journal for Numerical Methods in Engineering*, 71, 1466-1482.
- Melenk, J. M, & Babuska, I. (1996). The partition of unity finite element method: Basic theory and applications. *Computer Methods in Applied Mechanics and Engineering*, 139, 289-314.
- Miehe, C., & Gurses, E. (2007). A robust algorithm for configurational-force-driven brittle crack propagation with r-adaptive mesh alignment. *International Journal for Numerical Methods in Engineering*, 72, 127-155.

- Moës, N., Dolbow, J., & Belytschko, T. (1999). A finite element method for crack growth without remeshing. *International Journal for Numerical Methods in Engineering*, 46(1), 131-150.
- Moës, N., Dolbow, J., & Belytschko, T. (1999). A finite element method for crack growth without remeshing. *International Journal for Numerical Methods in Engineering*, 46, 131-150.
- Oliver, J., (1989). A consistent characteristic length for smeared cracking models. *International Journal for Numerical Methods in Engineering*, 28, 461-474.
- Rabczuk, T., & Belytschko, T. (2004). Cracking particles: a simplified meshfree method for arbitrary evolving cracks. *International Journal for Numerical Methods in Engineering*, 61(13), 2316-2343.
- Rabczuk, T., & Zi, G. (2007). A meshfree method based on the local partition of unity for cohesive cracks. *Computational Mechanics*, 39(6), 743-760.
- Sharan, M., Kansa, E. J., & Gupta, S. (1997). Application of the Multiquadric Method for Numerical Solution of Elliptic Partial Differential Equations. *Applied Mathematics and Computation*, 84, 275-302.
- Shibamura, K., Utsunomiya, T. (2008). PUFEM-based XFEM for avoiding the problem of blending elements. The 21st KKCNN Symposium on Civil Engineering, Singapore.
- Sukumar, N., Chopp, D. L., Moes, N., & Belytschko, T. (2001). Modeling holes and inclusions by level sets in the extended finite-element method. *Computer Methods in Applied Mechanics and Engineering*, 190, 6183-6200.
- Tarancon, J. E., Vercher, A., Giner, E., & Fuenmayor, F. J. (2009). Enhanced blending elements for XFEM applied to linear elastic fracture mechanics. *International Journal for Numerical Methods in Engineering*, 77, 126-148.
- Timon, R., Stephane, B., & Goangseup, Z. (2010). On three-dimensional modelling of crack growth using partition of unity methods. *Computers & Structures*, 88(23-24), 1391-1411.
- Ventura, G., Gracie, R., & Belytschko, T. (2009). Fast integration and weight function blending in the extended finite element method. *International Journal for Numerical Methods in Engineering*, 77, 1-29.
- Ventura, G., Xu, J. X., & Belytschko, T. (2002). Vector level set method and new discontinuity approximations for crack growth by EFG. *International Journal of Numerical Methods in Engineering*, 54(6), 923-944.
- Wu, Z. (1995). Compactly supported positive definite radial functions. *Advances in Computational Mathematics*, 4, 283-292.
- Wendland, H. (1998). Error estimates for interpolation by compactly supported radial basis functions of minimal degree. *Journal of Approximation Theory*, 93, 258-396.
- Wendland, H. (1995). Piecewise polynomial, positive definite and compactly supported radial basis functions of minimal degree. *Advances in Computational Mathematics*, 4, 389-396.



© 2018 by the authors; licensee Growing Science, Canada. This is an open access article distributed under the terms and conditions of the Creative Commons Attribution (CC-BY) license (<http://creativecommons.org/licenses/by/4.0/>).